Chinese Chemical Letters 33 (2022) 4705–4709

Contents lists available at ScienceDirect

Chinese Chemical Letters

journal homepage: www.elsevier.com/locate/cclet

Insight into the photoexcitation effect on the catalytic activation of H_2 and C-H bonds on TiO_2(110) surface

Min Zhou, Hai-Feng Wang*

Key Laboratory for Advanced Materials, Centre for Computational Chemistry and Research Institute of Industrial Catalysis, East China University of Science and Technology, Shanghai 200237, China

ARTICLE INFO

Article history:
Received 11 November 2021
Revised 24 December 2021
Accepted 27 December 2021
Available online 2 January 2022

Keywords:
Density functional theory calculation
Photocatalysis
H_2 activation
C-H bond activation
TiO_2

ABSTRACT

Semiconductor photocatalysis holds great promise for breaking the inert chemical bonds under mild condition; however, the photoexcitation-induced modulation mechanism has not been well understood at the atomic level. Herein, by performing the DFT+U calculations, we quantitatively compare H_2 activation on rutile TiO_2(110) under thermo- *versus* photo-catalytic condition. It is found that H_2 dissociation prefers to occur *via* the heterolytic cleavage mode in thermocatalysis, but changes to the homolytic cleavage mode and gets evidently promoted in the presence of photoexcited hole (h^+). The origin can be ascribed to the generation of highly oxidative lattice O-radical ($O_{br}^{\bullet-}$) with a localized unoccupied O-2p state. More importantly, we identify that this photo-induced promotion effect can be practicable to another kind of important chemical bond, *i.e.*, C–H bond in light hydrocarbons including alkane, alkene and aromatics; an exception is the C(sp^1)-H in alkyne (HC≡CH), which encounters inhibition effect from photoexcitation. By quantitative analysis, the origins behind these results are attributed to the interplay between two factors: C-H bond energy (E_{bond}) and the acidity. Owing to the relatively high E_{bond} and acidity, it favors the C(sp^1)-H bond to proceed with the heterolytic cleavage mode in both thermo- and photo-catalysis, and the photoexcited $O_{br}^{\bullet-}$ is adverse to receiving the transferred proton. By contrast, for the other hydrocarbons with moderate/low E_{bond}, the $O_{br}^{\bullet-}$ would enable to change their activation mode to a more favored homolytic one and evidently decrease the C–H activation barrier. This work may provide a general picture for understanding the photocatalytic R–H (R = H, C) bond activation over the semiconductor catalyst.

The activation of H–H and C–H bonds (classified as R-H, R = H, C) is of vital importance in the hydrogenation and dehydrogenation processes for the catalytic conversion and functionalization of saturated or unsaturated hydrocarbon compounds. Ways to efficiently break these chemical bonds under mild condition are always at the heart of chemical industry [1–3], which constitutes one of the foundations for the controllable formation of value-added commodity [4–6]. Generally, the catalytic cleavage and functionalization of R-H bond have been extensively explored on kinds of catalysts, such as the noble metals (Pt [7–9], Rh [10–12], Au [13,14] and *et al.* [15–18]), transition metal oxides (TMOs) and zeolites [19–21]. For example, the TMO-catalysts modified by single-atom metal doping or metal loading [22–26] were specifically manufactured to tailor the catalytic activity toward R-H bond activation. Despite these great progresses, these reactions are often performed at high temperatures (573–873 K) [27–29], which could lead to severe coke deposition and low product selectivity. Therefore, it is of paramount importance to develop more efficient catalysts or technologies for R-H bond activation under mild condition [30–33].

In this regard, the photocatalytic technology is believed to be capable of altering the reaction kinetics under mild condition owing to the presence of the excited carrier (h^+/e^-), and increasing experimental studies have demonstrated the feasibility for facilitating the R-H bond activation [34–36]. Taking the photocatalytic CH_4 activation as an example, it was proposed that CH_4 can be selectively converted to CH_3OH or HCHO under UV irradiation at room temperature over semiconductor catalysts, like TiO_2 [37], ZnO [38] and *et al.* [39–41]. However, the atomic-level insight into the photocatalytic effect is not unambiguously disclosed, to the best of our knowledge. Theoretically, owing to the difficulty in simulating photo-excited radicals properly on the semiconductor, the photocatalytic surface reaction has been relatively less studied with the detailed kinetic information provided [42–44]. It seems that most researches mainly focus on thermodynamic properties to evaluate the photocatalytic activity by considering the band structure of semiconductor and the potential of target reaction [45–48]. Kinetically, a comprehensive understanding of the nature

* Corresponding author.
E-mail address: hfwang@ecust.edu.cn (H.-F. Wang).

https://doi.org/10.1016/j.cclet.2021.12.074
1001-8417/

of photocatalytic effect on R-H bond activation at the atomic-scale level is very limited. Specifically, one may ask, how does the photoexcitation affect the H_2 and C-H activation, and what is the quantitative difference between thermo- and photo-catalytic mechanisms? Moreover, there are different types of C-H bonds, *e.g.*, C(sp^3)-H, C(sp^2)-H and C(sp^1)-H, and what are the general rule or difference of the photocatalytic effects on them?

Herein, we computationally explored the activation of H_2 molecule and diverse C–H bonds in thermo- and photo-catalysis on rutile TiO_2(110), one of the most studied semiconductors in photocatalysis. The theoretical results explicitly revealed the reaction mechanisms of H_2 activation; moreover, the activation of C-H bonds in diverse light-hydrocarbons, including acetylene (HC≡C–H), benzene (C_6H_5–H), ethylene (CH_2=CH–H), methane (CH_3–H), ethane (CH_3CH_2–H), propyne (CH≡CCH_2–H), toluene ($C_6H_5CH_2$–H) and propylene (CH_2=CHCH_2–H), were calculated and compared. The C–H bond energy (E_{bond}) and deprotonation energy (E_{dep}, corresponding to the acidity) were identified to be two main factors leading to the distinct behaviors of R–H bonds activation in thermo- and photo-excited conditions.

All spin-polarized DFT calculations were performed *via* Vienna ad initio Software Package (VASP) code [49,50], using the Perdew-Burke-Ernzerhof (PBE) functional within the generalized gradient approximation (GGA) [51,52]. The project-augmented wave (PAW) [53] method was used to represent the core-valence electron interaction, and the valence electronic states were expanded in plane wave basis sets with a cutoff energy of 450 eV. To ensure proper description of the valence electrons on Ti atom, a valence electron configurations $3p^6 4s^2 3d^2$ (small core) was applied.

We adopted a $p(3\times2)$ model of rutile TiO_2(110) with four TiO_2 atomic layers to accommodate the organic molecule and minimize the interaction between periodically repeated slabs. The vacuum between slabs was ~10 Å and a $2\times3\times1$ *k*-point mesh was used during the optimizations. The transition states (TSs) were searched by the constrained optimization scheme and were verified when (i) all forces on the atoms vanish and (ii) the total energy is a maximum along the reaction coordinate but a minimum with respect to the rest of the degrees of freedom [54–56]. All the atoms were allowed to relax, until the force on each atom was less than 0.05 eV/Å. The van der Waals forces was taken into account throughout this work to consider the possible weak interaction between intermediates and TiO_2(110) surface [57,58]. To model the photogenerated h^+/e^-, here we took the method of removing/adding electrons directly from the system with an additional neutralizing background charge applied in VASP due to the large dielectric constant of rutile TiO_2 [59]. Moreover, the photogenerated carriers usually tend to delocalize on TiO_2 system in GGA calculations due to the self-interaction error. To overcome this issue, DFT+*U* method with an on-site Coulomb interaction *U* added to the Ti-3d ($U=4.2$ eV) and O-2p orbitals ($U=6.3$ eV) was adopted for structure optimization and energy calculation [60], and the HSE06 hybrid functional was used to verify the electronic structure. Such an approach has been successfully applied to describe the photocatalytic reactions (*e.g.*, methanol oxidation, oxygen evolution reaction) on TiO_2 [61,62].

The adsorption energy of surface species (X) was defined as $E_{ad}(X)=E(X/sur)-E(sur)-E(X)$, where $E(sur)$, $E(X)$ and $E(X/sur)$ are the energy of catalyst surface, X species in the gas phase and X species adsorbed on the catalyst surface, respectively. Notably, at a specific temperature, the large entropy contributions of gaseous molecules were considered to estimate the adsorption free energy (G_{ad}) [63,64].

As Fig. 1a shows, the rutile TiO_2(110) surface is terminated by two types of unsaturated sites: two-fold coordinated bridge O and five-fold coordinated Ti (denoted as O_{br} and Ti_{5c}, respectively), which constitute the possible active centers for H-H and C-H bonds

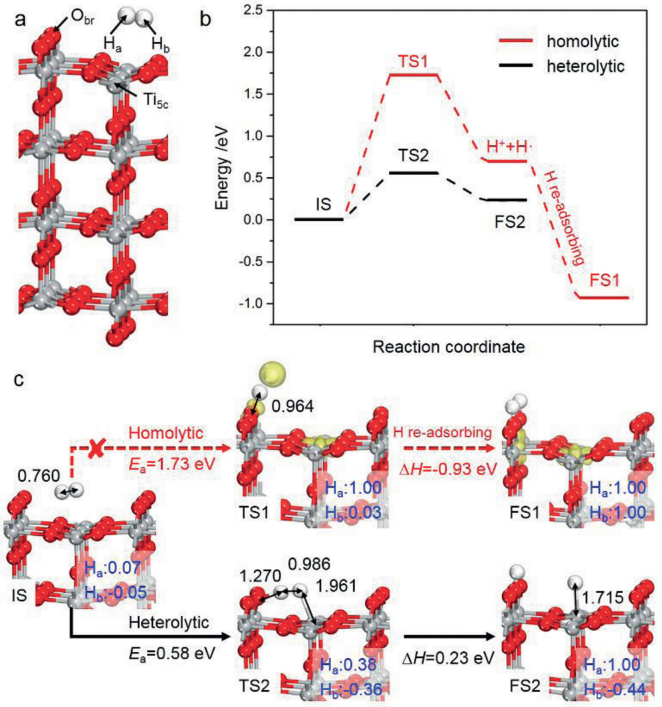

Fig. 1. (a) Ball-and-Stick model of rutile TiO_2(110) surface and H_2 adsorption configuration, in which H_a is the H atom approaching to O_{br} site and the other H atom is named as H_b. (b) Energy profiles of thermo-catalytic H_2 dissociation *via* homolytic and heterolytic modes, respectively, and (c) the optimized structures and spin density distribution of initial state (IS), transition state (TS) and final state (FS). The barrier (E_a) and enthalpy change (ΔH) are labeled (in eV). The distances of some key bonds and Bader charges of important intermediates are labeled in black (in Å) and blue (in |e|), respectively. Ti, gray; O, red; H, white.

activation. Firstly, the adsorption and dissociation of H_2 molecule under the thermocatalytic condition were briefly examined as a benchmark. It was found that H_2 can weakly adsorb on Ti_{5c} site with an adsorption energy, $E_{ad}(H_2)$, of −0.20 eV, which corresponds to an adsorption free energy, $G_{ad}(H_2)$, of 0.20 eV at room temperature. Subsequently, we tested two possible H_2 dissociation routes, including homolytic and heterolytic cleavage pathways, according to previous studies [30,31,65]. In the homolytic mode, H_2 activation is accompanied by the formation of a $H^·$ and a H^+ (*i.e.*, $H_2+Ti_{5c}{}^{4+}+O_{br}{}^{2-}\rightarrow H^{\bullet}+Ti_{5c}{}^{3+}+O_{br}H^-$); the activation barrier is as high as 1.73 eV and the enthalpy change reaches 0.70 eV (see energy profiles in Fig. 1b). Alternatively, when the reaction proceeds *via* the heterolytic cleavage mode, which synergistically occurs at the O_{br} and Ti_{5c} dual sites (*i.e.*, $H_2+Ti_{5c}{}^{4+}+O_{br}{}^{2-}\rightarrow Ti_{5c}{}^{4+}$-$H^-+O_{br}H^-$), the barrier decreases a lot to 0.58 eV. This indicates that the heterolytic mode is energetically more favorable for H-H bond scission than the homolytic mode. Moreover, the H atoms dissociated from the heterolytic cleavage would be eventually captured by O_{br} and Ti_{5c} sites yielding a H^+ and a H^- anion, evidenced by their Bader charges of 1.00 |e| and −0.44 |e| (Fig. 1c), respectively. Notably, these barriers are slightly higher than those reported by Hu *et al.* (1.39 eV and 0.37 eV in homolytic and heterolytic modes, respectively), owing to the self-interaction error of TiO_2 system ignored in their study [65].

Secondly, we calculated the photocatalytic H_2 dissociation on TiO_2(110) surface. Generally, the generated photohole/electron pairs under light illumination thermodynamically tend to be trapped by O_{br} and Ti_{5c} sites and form $O_{br}{}^{\bullet-}$ and $Ti_{5c}{}^{3+}$, respectively, corresponding to $O_{br}{}^{2-}+h^+\rightarrow O_{br}{}^{\bullet-}$ and $Ti_{5c}{}^{4+}+e^-\rightarrow Ti_{5c}{}^{3+}$ [66–68]. As Figs. 2a and b show, our calculations verify that these two excited active sites ($O_{br}{}^{\bullet-}$ and $Ti_{5c}{}^{3+}$)

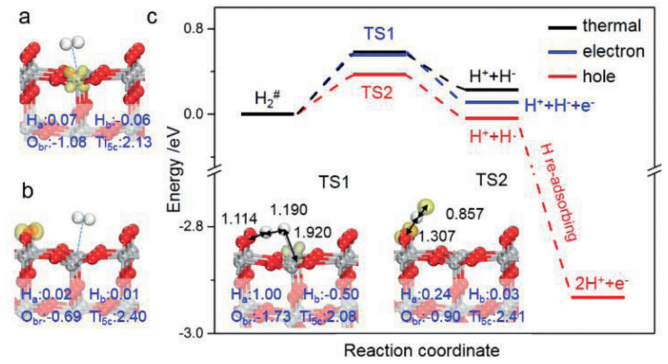

Fig. 2. (a, b) H_2 adsorption on TiO_2(110) in the presence of Ti_{5c}^{3+} and $O_{br}^{\bullet-}$, respectively. (c) Energy profiles of H_2 dissociation in thermocatalysis *via* heterolytic mode (black line) or under light irradiation, including hole- and electron-assisted circumstances (red and blue lines, respectively).

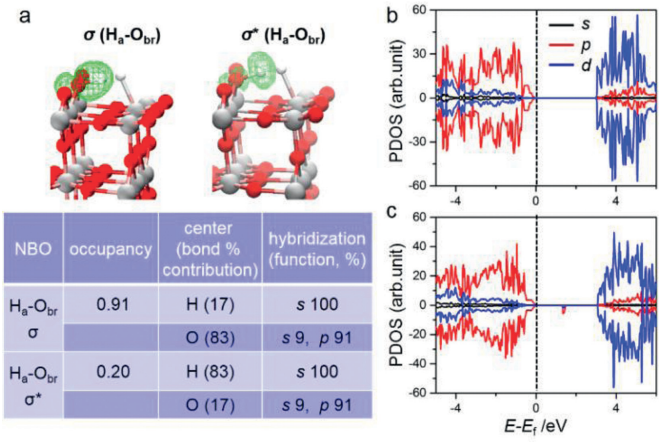

NBO	occupancy	center (bond % contribution)	hybridization (function, %)
H_a-O_{br} σ	0.91	H (17)	*s* 100
		O (83)	*s* 9, *p* 91
H_a-O_{br} σ*	0.20	H (83)	*s* 100
		O (17)	*s* 9, *p* 91

Fig. 3. (a) The periodic natural bond orbital (NBOs) of TS for H_2 dissociation in thermocatalysis *via* the heterolytic mode. (b, c) The projected densities of states (PDOSs) of pristine TiO_2(110) and hole-trapping TiO_2(110), respectively, using HSE06. The vertical dotted lines in the PDOSs denote the fermi levels.

have insignificant effect on H_2 adsorption with $E_{ad}(H_2)$ of −0.22 eV and −0.21 eV, respectively. With the assistance of Ti_{5c}^{3+}, the barrier of H_2 dissociation is nearly the same as that in thermocatalysis (0.56 eV *vs.* 0.58 eV) with a very similar TS structure (see TS1 in Fig. 2c), implying little contribution of photo-electron on H_2 activation. Intriguingly, on hole-trapped TiO_2(110) surface, the TS of H-H bond cleavage changes from the dihapto configuration in the thermocatalytic condition to the monohapto one (Figs. 2c and 1c), and the barrier is reduced to 0.37 eV with an enthalpy change of −0.04 eV (*i.e.*, $H_2 + O_{br}^{\bullet-} \rightarrow HO_{br}^{-} + H^{\bullet}$). Notably, in comparison with the pristine homolytic cleavage mode in thermocatalysis, the barrier has largely declined (1.73 eV *vs.* 0.37 eV). With the generation of $H^{\bullet}$ radical, it would further re-adsorb on O_{br} and form H^+ with a large energy release (−2.90 eV). More specifically, in this photocatalytic TS, one H in H_2 molecule is captured by $O_{br}^{\bullet-}$ and the other H suspends above the TiO_2 surface with the H···H and H_a···O_{br} bonds being 0.857 Å and 1.307 Å, respectively. In other word, it exhibits a radical-like TS, and the radical nature of H atom is also confirmed by Bader spin charge of 0.97 |e|. Therefore, the H-H bond activation mediated by photo-hole essentially follows the homolytic cleavage mechanism.

To shed light on the promotion effect of photo-hole on H_2 dissociation, we quantitatively inspected the related electronic structure information. Firstly, the periodic natural bond orbital (NBO) [69] of two-site assisted TS complex in thermocatalysis was analyzed to uncover the bonding/antibonding nature of H_a-O_{br} and H_b-Ti_{5c} (see Fig. 3a), in which H_a/H_b denotes the H atom in H_2 close to the O_{br}/Ti_{5c} site, respectively (Fig. 1a). Quantitatively, the charge of H_a is calculated to be 0.65 |e| in the H_2 activation TS, indicating that the electron in H_a is partially shared by the forming H_a-O_{br} bond; however, it owns a charge of 1.06 |e| for the H_b atom in H_b-Ti_{5c} bond, implying the negligible electron transfer (*versus* that (0.93 |e|) of H_b atom in pristine H_2 molecule). Moreover, the occupancy of H_a-O_{br} bonding/antibonding is 0.91/0.20 |e|, but nearly zero for H_b-Ti_{5c} bond. Therefore, we can speculate that the activation of H_2 molecule depends mainly on the O_{br} site, whereas the Ti_{5c} site contributes to a small extent, which could well explain the greater promotion effect of photo-hole than photo-electron. Similar result can be drawn in the C-H bond activation of CH_4 molecule on rutile TiO_2(110) surface [70].

Furthermore, the projected densities of states (PDOSs) of TiO_2(110) in the absence or presence of $O_{br}^{\bullet-}$ were calculated (see Figs. 3b and c). It can be seen that the presence of localized photo-hole does not lead to significant change in the whole band gap, but induces a new unoccupied state within the forbidden band. In principle, this hole-state is conductive to accepting electron and exhibits strong oxidizability, evidenced by the higher energy level of $O_{br}^{\bullet-}$ (~1.5 eV above the fermi level). In this sense, the superior performance of $O_{br}^{\bullet-}$ than O_{br}^{2-} on H-H bond rupture can be rationalized as follows. $O_{br}^{\bullet-}$ holds less electron (−0.69 |e|) than O_{br}^{2-} (−1.08 |e|), and this reactive $O_{br}^{\bullet-}$ site, as a stronger oxidative center, can more easily accept electron from the dissociated hydrogen atom after H_2 homolytic cleavage in photocatalysis, thereby largely decreasing the activation barrier.

With the understanding of photoexcitation effect on modulating H_2 dissociation, we are now at the position to explore the C-H bond activation in a series of different organic molecules on TiO_2(110), aiming to uncover the general rule of the photo-hole effect, which includes (i) sp^1–C group: HC≡C–H; (ii) sp^2–C group: C_6H_5–H and CH_2=CH–H; (iii) sp^3–C group: CH_3–H, CH_3CH_2–H, CH≡CCH_2–H, $C_6H_5CH_2$–H and CH_2=$CHCH_2$–H. At first, the thermally-driven C–H bond activation processes were studied. By comparing the barriers in homolytic and heterolytic cleavage modes (Table 1), we can see that heterolytic route is not always the most favorable one for all C-H bonds, which differs from H–H bond activation. In detail, the HC≡C-H, C_6H_5–H, CH_2=CH–H, CH_3–H and CH_3CH_2–H bonds prefer to be activated *via* the heterolytic cleavage mode, whereas the homolytic mode for the others (*i.e.*, CH≡CCH_2–H, $C_6H_5CH_2$–H and CH_2=$CHCH_2$–H) (Fig. 4a and Table 1). Additionally, except for HC≡C–H (0.13 eV), almost all the reaction barriers of the most favored pathway are above 0.90 eV, which indicates

Table 1
Reaction barriers (E_a) of various R-H bonds cleavage on TiO_2(110) in thermo- and photo-catalysis (heterolysis/homolysis, abbreviated as hetero-/homo-, respectively). E_{bond} is the R-H bond energy defined with the reaction energy of homolytic process (R-H → R$^{\bullet}$ + H$^{\bullet}$) and E_{dep} is the deprotonation energy from the heterolytic process (R-H → R^- + H^+), taken from the NIST WebBook [71]. Note that the TSs of photocatalysis in heterolytic mode are hardly accessible in geometry, and thus their barriers are not shown here. The unit is eV.

R-H		E_a (thermal)		E_a (hole)		E_{bond}	E_{dep}
		hetero-	homo-	hetero-	homo-		
	H-H	0.58	1.73	/	0.37	4.53	17.36
group-I	C_6H_5–H	0.90	1.96	/	0.52	4.93	17.40
	CH_2CH–H	1.02	1.82	/	0.50	4.88	17.66
	CH_3–H	1.12	1.83	/	0.29	4.72	17.99
	CH_3CH_2–H	1.35	1.61	/	0.23	4.50	18.22
group-II	CH≡CCH_2–H	1.64	1.42	/	0.06	3.98	16.49
	C_6H_5–CH_2–H	1.46	1.25	/	0.02	3.97	16.45
	CH_2=$CHCH_2$–H	1.55	1.17	/	0.10	3.85	16.96
group-III	HC≡C–H	0.13	2.10	0.78	1.07	5.92	16.38
	CH_3O–H, Ref. [61]	0.17	/	0.60	/	4.58	16.55

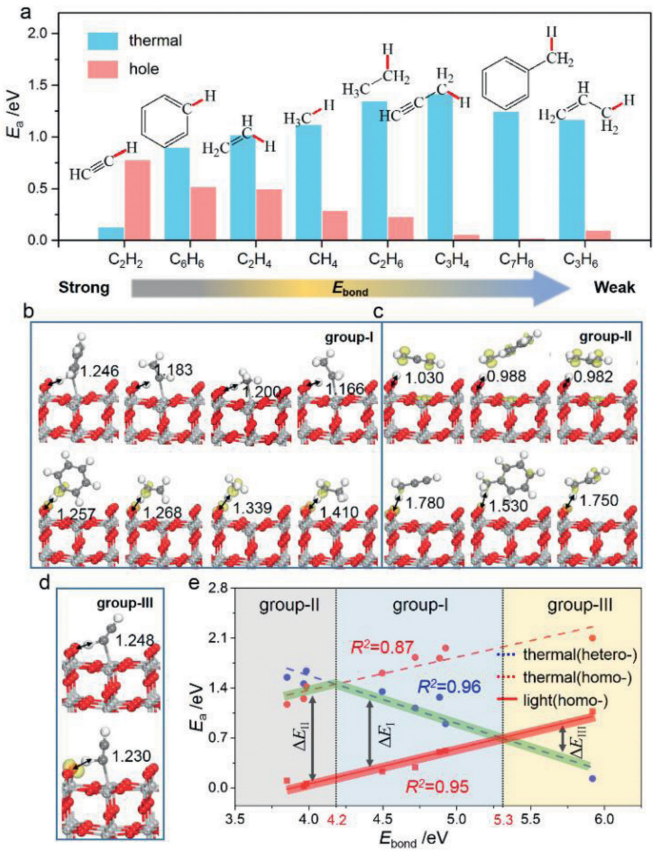

Fig. 4. (a) Comparisons for the most favored activation barrier (E_a) of C-H bonds in the thermal and photo-hole assisted conditions, as well as the corresponding TSs for group-I, -II and -III C-H bonds (b-d), respectively, in which the distances of $H_a\cdots O_{br}$ bonds are labeled in black (in Å). (e) Correlations between E_a and E_{bond} in the thermal and photo-hole assisted conditions, respectively.

the difficulty of C–H bond activation at room temperature. In the presence of $O_{br}^{\bullet-}$, we identified that the homolytic mode becomes more favored for C–H bonds in all but HC≡C–H (Table 1). Particularly, the activation barriers for the $CH{\equiv}CCH_2$–H, $C_6H_5CH_2$–H and $CH_2{=}CHCH_2$–H bonds are extremely small (< 0.10 eV) as compared to those in the thermocatalytic condition; for the usually-known inert C–H bonds in benzene, ethylene and methane, the barriers can also be reduced to below 0.52 eV. Overall, these results imply that for all these C–H bond in light hydrocarbons, the photo-hole can prompt their activation evidently, except for HC≡CH molecule.

In addition, it is remarkable that the activation of these C–H bonds exhibits different behaviors, and is modulated by $O_{br}^{\bullet-}$ to different degrees in comparison to the thermocatalysis (Fig. 4a). According to the results revealed above, these C–H bonds may be, therefore, classified as three groups: (group-I) the ones (CH_3–H, CH_3CH_2–H, CH_2=CH–H and C_6H_5–H, Fig. 4b) that follow the heterolysis mode in thermocatalysis and change to the homolysis mode in photocatalysis, to which the photo-effect is beneficial (see ΔE_I in Fig. 4e); (group-II) the ones ($CH{\equiv}CCH_2$–H, $C_6H_5CH_2$–H and $CH_2{=}CHCH_2$–H, Fig. 4c) that follow the homolysis mode in thermocatalysis and keep it in photocatalysis, where the photo-effect is more efficient than group-I (see ΔE_{II} in Fig. 4e); (group-III) HC≡C–H (Fig. 4d), which prefers the heterolysis mode in both thermo- and photo-catalysis, and the presence of $O_{br}^{\bullet-}$ will inhibit the HC≡C–H bond activation (see ΔE_{III} in Fig. 4e). One may naturally ask, what are the origins for these three different behaviors? Specifically, why do the group-II C–H bonds tend to follow the homolytic cleavage mode, differing from the others? For HC≡C–H, why does it always follow the heterolysis mode, and why is the presence of $O_{br}^{\bullet-}$ adverse to its C–H bond scission?

Toward these questions, firstly, we quantitatively tested the dependence of the E_a values *via* homolytic/heterolytic routes in the thermocatalytic condition on the corresponding C–H bond energies (E_{bond}). Two overall linear relations can be obtained with R^2 of 0.87/0.96 (Fig. 4e), respectively. More intriguingly, as E_{bond} increases, E_a in the homolytic route increases, but decreases in the heterolytic one, and the crossing point of the two curves is at $E_{bond} = 4.2$ eV. These correlations clearly suggest that the choice of homolysis *versus* heterolysis in the thermocatalytic condition strongly depends on the C–H bond energy: the heterolysis is favored in the strong bond-energy region, while the homolysis is preferred in weak bond-energy region. For the group-II C–H bonds, they own the relatively weaker E_{bond} among all the studied ones (Table 1), due to the stability of dehydrogenated molecule-fragment (*i.e.*, $CH{\equiv}C\text{-}CH_2^{\bullet}$, C_6H_5–$CH_2^{\bullet}$ and $CH_2{=}CH\text{-}CH_2^{\bullet}$) with extended π-electron conjugation, which rationalizes the preference of homolytic cleavage in thermocatalysis.

With the participation of $O_{br}^{\bullet-}$ in the C–H bond activation, a similar linear correlation exists between the E_a following the homolysis mode in the photocatalytic condition and E_{bond} as well ($R^2 = 0.95$, Fig. 4e). One can see from Fig. 4e that this line is overall downward shift in parallel as compared to that of the homolysis mode in the thermocatalytic condition, which again illustrates the promotion effect originating from the high oxidizability of $O_{br}^{\bullet-}$. Accordingly, we can explain the different promotion effect of $O_{br}^{\bullet-}$ on the C–H bonds of group-I *versus* group-II, which gives $\Delta E_{II} > \Delta E_I$. For group-II C–H bonds, the homolytic mode is favored in both thermo- and photo-catalytic conditions, and the promotion extent (ΔE_{II}) of $O_{br}^{\bullet-}$ is the largest as seen from Fig. 4e. Differently, for group-I C–H bonds, the heterolysis mode is more favored in the thermocatalytic condition, and it will change to the homolysis mode in photocatalysis; thus, the photo-promotion effect (ΔE_I) is relatively weakened relative to ΔE_{II}. Moreover, it is worth noting that ΔE_I becomes smaller and smaller as the E_{bond} increases.

Secondly, as illustrated in Fig. 4e, with the increase of E_{bond}, we can see that the thermodynamically driven heterolytic mode becomes more and more feasible. When above ~5.3 eV, it will be even more favored than the photo-driven process, essentially ascribed to that the localized hole at $O_{br}^{\bullet-}$ cannot provide enough energy to compensate the C–H bond energy. Specifically for HC≡C–H activation, the large E_{bond} of HC≡C–H is unfavorable for the occurring of homolytic mode. Moreover, as we know, HC≡CH together with the group-II molecules ($CH{\equiv}CCH_3$, C_6H_5-CH_3 and $CH_2{=}CHCH_3$) displays weak acidity [72,73], consistent with their relatively small deprotonation energies (E_{dep}) in Table 1. These two factors imply that the HC≡C–H is more susceptible to releasing hydrogen in the form of proton (*i.e.*, $HC{\equiv}C{-}H \rightarrow HC{\equiv}C^- + H^+$). In this circumstance, the hydrogen in HC≡C–H would more easily combine with the O_{br}^{2-} site *via* heterolysis rather than homolysis, which accordingly corresponds to a lower barrier of 0.13 eV (2.10 eV in homolysis). When the $O_{br}^{\bullet-}$ is present, owing to the additional Coulomb repulsion between positively charged H^+ and $O_{br}^{\bullet-}$ (*versus* that in $H^+\cdots O_{br}^{2-}$), the activation process is kinetically less favored than that in the pristine O_{br}^{2-} (0.78 eV *vs.* 0.13 eV in photo- and thermo-catalysis, respectively). Thus, the HC≡C–H bond prefers to be activated through the heterolytic mode and photo-hole would suppress this activation process, as a result of its strong bond energy and acidity. Notably, the similar result was also observed in the heterolytic O–H bond cleavage in the photocatalytic CH_3OH oxidation revealed in our previous study (Table 1) [61].

In summary, we have quantitatively studied the activation mechanism of H_2 and a series of C–H bonds on TiO_2(110) in the thermo- and photo-catalytic conditions, aiming to reveal the

general photoexcitation effect on modulating the chemical bonds breakage. The main results can be summarized as follows:

(i) The thermal-driven H_2 activation on $TiO_2(110)$ tends to obey the heterolytic cleavage mode, and the $O_{br}^{\bullet-}$ radical formed from the photo-hole localization would change the mode to be homolytic one and evidently facilitate the activation process.

(ii) We identified that the examined C–H bonds can be classified as three groups in terms of the bond energy and acidity: group-I (CH_3–H, CH_3CH_2–H, CH_2=CH–H and C_6H_5–H), group-II (CH≡CCH_2–H, $C_6H_5CH_2$–H and CH_2=$CHCH_2$–H) and group-III (HC≡C–H). The bond energy order is group-II < group-I < group-III; meanwhile, group-II/-III C–H bonds own weak acidity. The $O_{br}^{\bullet-}$ species can facilitate the activation of group-I/II C–H bonds to different degrees, whereas inhibits the one in HC≡C–H.

(iii) The different C–H activation behaviors in group-I to group-III could be largely attributed to the C–H bond energies and acidities. For the group-I/-II C–H bonds with relatively moderate/low bond energies, they obey the heterolytic/homolytic cleavage mechanism in thermocatalysis, and will uniformly obey the homolysis mechanism driven and simultaneously promoted by the highly oxidative $O_{br}^{\bullet-}$, where the promotion effect on group-II C–H bonds is more evident with nearly negligible barriers.

(iv) Owing to the strong bond energy and weak acidity, we found that the HC≡C–H bond consistently prefers to be activated *via* the heterolytic cleavage mode, and $O_{br}^{\bullet-}$ would inhibit this activation as a result of additional Coulomb repulsion between the dissociated proton and $O_{br}^{\bullet-}$ (*versus* the pristine O_{br}^{2-} on $TiO_2(110)$).

This work provided a general atomic-level description on the photo- *versus* thermo-catalytic activation of H_2 and various C–H bonds, which may explicitly deepen our understanding of the photocatalytic effect on modulating the chemical bonds breakage.

Declaration of competing interest

The authors report no declarations of interest.

Acknowledgments

This project was supported by National Nature Science Foundation of China (Nos. 21873028, 91945302), National Ten Thousand Talent Program for Young Top-notch Talents in China, Shanghai Shu-Guang project (No. 17SG30), and the Fundamental Research Funds for the Central Universities

References

[1] R. Khorasani, P.E. Fleming, Comput. Theor. Chem. 1096 (2016) 89–93.
[2] J. Berkowitz, G.B. Ellison, D. Gutman, J. Phys. Chem. 98 (1994) 2744–2765.
[3] B.B. Wayland, Polyhedron 7 (1988) 1545–1555.
[4] L. Meng, Z. Chen, Z. Ma, et al., Energy Environ. Sci. 11 (2018) 294–298.
[5] X. Li, W. Wang, F. Dong, et al., ACS Catal. 11 (2021) 4739–4769.
[6] M. Huš, D. Kopač, B. Likozar, J. Catal. 386 (2020) 126–138.
[7] J.L. Gland, G.B. Fisher, E.B. Kollin, J. Catal. 77 (1982) 263–278.
[8] G.E. Gdowski, R.J. Madix, Surf. Sci. 119 (1982) 184–206.
[9] R. Van Lent, S.V. Auras, K. Cao, et al., Science 363 (2019) 155–157.
[10] X. Qi, Y. Li, R. Bai, et al., Acc. Chem. Res. 50 (2017) 2799–2808.
[11] S.R. Neufeldt, G. JiméNez-Osés, J.R. Huckins, et al., J. Am. Chem. Soc. 137 (2015) 9843–9854.
[12] J.C. Lewis, R.G. Bergman, J.A. Ellman, Acc. Chem. Res. 41 (2008) 1013–1025.
[13] M. Wijzenbroek, D. Helstone, J. Meyer, et al., J. Chem. Phys. 145 (2016) 144701.
[14] Q. Wu, L. Zhou, G.C. Schatz, et al., J. Am. Chem. Soc. 142 (2020) 13090–13101.
[15] S. Mukherjee, F. Libisch, N. Large, et al., Nano Lett. 13 (2013) 240–247.
[16] T. Engel, H. Kuipers, Surf. Sci. 90 (1979) 181–196.
[17] D.F. Padowitz, S.J. Sibener, Surf. Sci. 254 (1991) 125–143.
[18] Y. Sun, S. Zhang, W. Zhang, et al., Chin. J. Chem. Phys. 31 (2018) 485–491.
[19] F. Zaera, D. Chrysostomou, Surf. Sci. 457 (2000) 89–108.
[20] M. L.Yang, Y.A. Zhu, C. Fan, et al., Phys. Chem. Chem. Phys. 13 (2011) 3257–3267.
[21] Y. Chen, D.G. Vlachos, J. Phys. Chem. C 114 (2010) 4973–4982.
[22] W. Zhang, M. Pu, M. Lei, Langmuir 36 (2020) 5891–5901.
[23] G. Righi, R. Magri, A. Selloni, J. Phys. Chem. C 123 (2019) 9875–9883.
[24] L. Brugnoli, A. Pedone, M.C. Menziani, et al., J. Phys. Chem. C 123 (2019) 25668–25679.
[25] Y. Chen, P. Hu, M.H. Lee, et al., Surf. Sci. 602 (2008) 1736–1741.
[26] Y. Chen, J. Cheng, P. Hu, et al., Surf. Sci. 602 (2008) 2828–2834.
[27] M.V. Bossche, H. Gronbeck, J. Am. Chem. Soc. 137 (2015) 12035–12044.
[28] F. Zasada, J. Janas, W. Piskorz, et al., ACS Catal. 7 (2017) 2853–2867.
[29] Z. Zhu, W. Guo, Y. Zhang, et al., Carbon Energy 3 (2021) 519–540.
[30] T. Whittaker, K.B.S. Kumar, C. Peterson, et al., J. Am. Chem. Soc. 140 (2018) 16469–16487.
[31] K. Sun, M. Kohyama, S. Tanaka, et al., J. Phys. Chem. C 118 (2014) 1611–1617.
[32] S. Mukherjee, L. Zhou, A.M. Goodman, et al., J. Am. Chem. Soc. 136 (2014) 64–67.
[33] N. Yodsin, C. Rungnim, S. Tungkamani, et al., J. Phys. Chem. C 124 (2019) 1941–1949.
[34] Y. Chen, S. Ji, W. Sun, et al., Angew. Chem. Int. Ed. 132 (2020) 1295–1301.
[35] H. She, H. Zhou, L. Li, et al., ACS Sustain. Chem. Eng. 6 (2018) 11939–11948.
[36] T. Yan, Y. Wang, Y. Cao, et al., Appl. Catal. A: Gen. 630 (2022) 118457.
[37] C.F. Lien, M.T. Chen, Y.F. Lin, et al., J. Chin. Chem. Soc. 51 (2004) 37–42.
[38] H. Song, X. Meng, S. Wang, et al., J. Am. Chem. Soc. 141 (2019) 20507–20515.
[39] X. Cao, T. Han, Q. Peng, et al., ChemComm 56 (2020) 13918–13932.
[40] P.V.L. Reddy, K.H. Kim, H. Song, Renew. Sustain. Energy Rev. 24 (2013) 578–585.
[41] N. Feng, H. Lin, H. Song, et al., Nat. Commun. 12 (2021) 4652.
[42] R. Sun, C. He, L. Fu, et al., Chin. Chem. Lett. 33 (2022) 527–532.
[43] L. Fu, R. Wang, C. Zhao, et al., Chem. Eng. J. 414 (2021) 128857.
[44] J. Yu, C. He, C. Pu, et al., Chin. Chem. Lett. 32 (2021) 3149–3154.
[45] Y. Zhao, W. Gao, S. Li, et al., Joule 3 (2019) 920–937.
[46] Y. Tian, L. Piao, X. Chen, Green Chem. 23 (2021) 3526–3541.
[47] W.B. Jiang, J.X. Low, et al., J. Univ. Sci. Technol. China 50 (2020) 1361.
[48] M. Harb, G. Jeantelot, J.M. Basset, J. Phys. Chem. C 123 (2019) 28210–28218.
[49] G. Kresse, J. Furthmüller, Phys. Rev. B 54 (1996) 11169.
[50] G. Kresse, J. Furthmüller, Comput. Mater. Sci. 6 (1996) 15–50.
[51] J.P. Perdew, A. Ruzsinszky, G.I. Csonka, Phys. Rev. Lett. 100 (2008) 136406.
[52] J.P. Perdew, K. Burke, M. Ernzerhof, Phys. Rev. Lett. 77 (1996) 3865.
[53] G. Kresse, D. Joubert, Phys. Rev. B 59 (1999) 1758.
[54] H. Yuan, H. Yang, P. Hu, et al., ACS Catal. 11 (2021) 6835–6845.
[55] H.F. Wang, D. Wang, X. Liu, et al., ACS Catal. 6 (2016) 5393–5398.
[56] H.F. Wang, R. Kavanagh, Y.L. Guo, et al., Angew. Chem. Int. Ed. 51 (2012) 6657–6661.
[57] S. Grimme, J. Comput. Chem. 27 (2006) 1787–1799.
[58] S. Grimme, J. Antony, S. Ehrlich, et al., J. Chem. Phys. 132 (2010) 154104.
[59] M. Setvin, C. Franchini, X. Hao, et al., Phys. Rev. Lett. 113 (2014) 086402.
[60] D. Wang, H.F. Wang, P. Hu, Phys. Chem. Chem. Phys. 17 (2015) 1549–1555.
[61] J. Zhang, C. Peng, H. Wang, et al., ACS Catal. 7 (2017) 2374–2380.
[62] D. Wang, T. Sheng, J. Chen, et al., Nat. Catal. 1 (2018) 291–299.
[63] H. Yuan, N. Sun, J. Chen, et al., ACS Catal. 8 (2018) 9269–9279.
[64] H. Yuan, J. Chen, H. Wang, et al., ACS Catal. 8 (2018) 10864–10870.
[65] G. Hu, Z. Wu, D.E. Jiang, J. Phys. Chem. C 122 (2018) 20323–20328.
[66] J. Zhang, P. Zhou, J. Liu, et al., Phys. Chem. Chem. Phys. 16 (2014) 20382–20386.
[67] S. Wu, L. Wang, J. Zhang, J. Photochem. Photobiol. C Photochem. Rev. 46 (2021) 100400.
[68] H. Sheng, Q. Li, W. Ma, et al., Appl. Catal. B 138 (2013) 212–218.
[69] B.D. Dunnington, J.R. Schmidt, J. Chem. Theory Comput. 8 (2012) 1902–1911.
[70] M. Zhou, H.F. Wang, JACS Au. 2 (2022) 188–196.
[71] P.J. Linstrom, W.G. Mallard, Chem. Eng. 46 (2001) 1059–1063.
[72] P. Pässler, W. Hefner, K. Buckl, et al., Ullmann's Encyclopedia of Industrial Chemistry, Wiley-VCH, Weinheim, 2000.
[73] K.M. Ervin, S. Gronert, S.E. Barlow, et al., J. Am. Chem. Soc. 112 (1990) 5750–5759.